LIDAR-BASED TERRAIN MAPPING AND NAVIGATION FOR A PLANETARY EXPLORATION ROVER

Genya Ishigami, Masatsugu Otsuki, and Takashi Kubota

Institute of Space and Astronautical Science, Japan Aerospace Exploration Agency
Yoshinodai 3-1-1, Sagamihara, Kanagawa, 252-5210, Japan
e-mail: ishigami.genya@jaxa.jp

ABSTRACT

This paper presents a terrain mapping and path planning techniques for a planetary exploration rover. A light detection and ranging (LIDAR) is employed in this work to obtain a point cloud data of the terrain feature. A terrain map converted from the point cloud data is represented with a sector-shaped reference grid, resulting in a digital elevation map with the cylindrical coordinate, called C^2DEM. The path planning uses a cost function composed of terrain inclination, terrain roughness, and path length to generate a route for safer travel. A multi-path planning method with a quantitative evaluation of multiple candidate paths is also proposed to find the most feasible path between the candidates. Field experiments with a rover prototype at a Lunar/Martian analog site confirms the usefulness of the proposed techniques including the LIDAR-based terrain mapping and the multi-path planning method.

Key words: LIDAR, planetary exploration rover, autonomous mobility, terrain mapping, and path planning.

1. INTRODUCTION

The natural rough terrain on the Moon or Mars requires a planetary exploration rover to evade mobility hazards, which includes vehicle rollover on sloped terrain, or immobilizing wheel slippage on loose sand. However, a prior knowledge of physical characteristics of the environment is hardly available. Therefore, the rover needs to have a high degree of autonomous mobility that enables the rover to navigate itself by sensing a terrain environment as well as planning a feasible path for rough terrain traverse.

A terrain feature information can be exploited to assess obstacle size, slope angle, or terrain roughness so that the rover is able to find its heading for travel. The rover uses visual information obtained from an onboard stereoscopic camera to measure terrain features [1]–[4]. The drawbacks of the camera-based terrain mapping are that a stereo matching process is generally a time-consuming task for the low-power flight CPU of the rover, requiring relatively long computational time [3]. Additionally, the quality of visual information may vary with the intensity of sunlight/shadows.

Another technique for the terrain mapping involves the use of a light detection and ranging (LIDAR) that can determine a distance from a laser emitter to an object based on the time of flight principle. There have been an extensive research and development for using the LIDAR technique in a terrain feature mapping and terrain classification [5]–[8]. Comparing the LIDAR-based terrain mapping to the camera-based one, the LIDAR can directly measure three-dimensional distances from the sensor to the objects, providing "point cloud" data of the scene without any additional processes (c.f. the camera-based mapping needs stereo matching for the 3D mapping).

The primary scope of this paper is to develop a LIDAR-based terrain mapping and path planning strategy for a planetary exploration rover. A two-dimensional scanning LIDAR with a rotatable stage is used to realize three-dimensional mapping. The point cloud data of the terrain features provided by the LIDAR are converted into a digital elevation map with a sector-shaped reference grid, resulting in an elevation map with cylindrical coordinates, called C^2DEM. The terrain mapping with the C^2DEM achieves detailed representation of the terrain near the rover as well as wide selectivity of the rover look-ahead directions. The path planning algorithm in this work considers three indices: terrain inclination, terrain roughness, and path length. A cost function, composed of these indices with varied weighting factors, generates various "candidate" paths on the map. A multi-path planning method described in this paper performs extensive exploration of the weighting factors and quantitatively examines these candidate paths to find the most feasible path between the candidates. The selected path is discretized into several way points, which contain relative distances and headings from one to another. The rover then travels through each waypoint until it reaches a designated goal. Field experiments with a rover prototype were performed at a Lunar/Martian analog terrain to evaluate the usefulness of the LIDAR-based terrain mapping and path planning strategy.

Table 1. Specification of the LIDAR scanning system

Measurable distance	$\sim$ 0.1 – 30 m
Accuracy (distance)	$\pm$ 0.1 m
Scanning range	$\pm$ 95 deg
Scanning angle resolution	0.25 deg
Tilting range	0 to 60 deg
Tilt angle resolution	0.33 deg

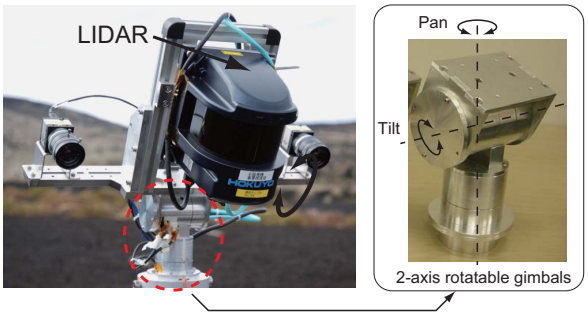

Figure 1. Gimbaled-LIDAR system for terrain mapping

This paper is organized as follows: Section 2 describes the terrain mapping with the LIDAR; Section 3 explains the path planning method; and the experimental tests are summarized in Section 4.

2. TERRAIN MAPPING WITH A LIDAR

2.1. LIDAR Scanning System

The LIDAR used for terrain mapping is UXM-30 LX-E[1] developed by Hokuyo Corp. [9]. This LIDAR is mounted on the gimbals (Fig. 1). Controlling the tilting motion of the gimbals, along with the two-dimensional scanning of the LIDAR, three-dimensional terrain mapping is achieved. The LIDAR provides a terrain feature as a set of point cloud data. A three dimensional location of each scanned point can be calculated by the distance measured with respect to the scanning angle and the tilting angle. The specification of the LIDAR system is summarized in Tab. 1.

2.2. Cylindrical Coordinate DEM (C^{2}DEM)

Terrain features are often represented by a digital elevation map (DEM) that is defined by a series of elevations along with discrete nodes. A conventional DEM usually employs a square-shaped reference grid for the conversion from a point cloud data to the DEM. Then, the elevation of each node in the reference grid is determined from the point with the highest elevation among multiple points inside the grid. Applying this process to the entire point cloud data set, the DEM is obtained.

[1]The LIDAR used in this work is not space-hardened.

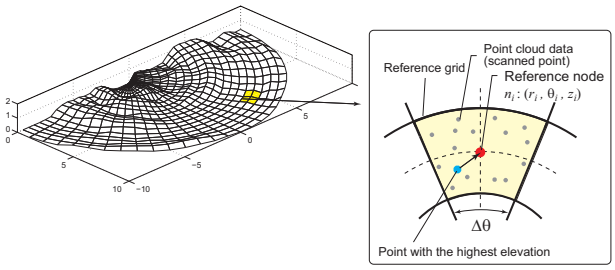

Figure 2. Cylindrical Coordinate DEM (C^{2}DEM)

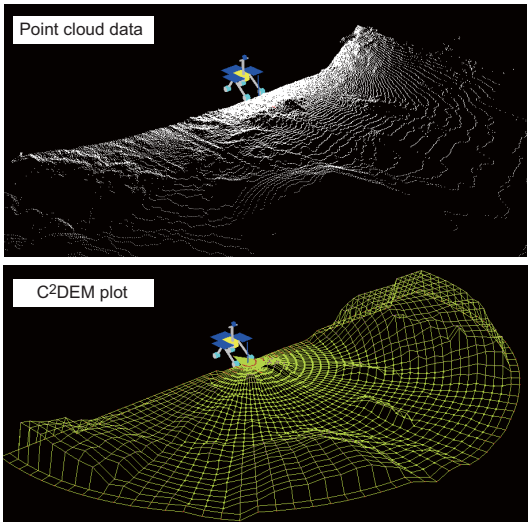

Figure 3. An example of the C^{2}DEM conversion from point cloud data

The point cloud data that are obtained from the LIDAR usually has high resolution (dense) for the points near the rover, and low resolution (sparse) for the points that are far from the rover. To represent these characteristics of the point cloud data, this paper proposes a sector-shaped reference grid for the DEM conversion, which is represented in the cylindrical coordinate, termed as C^{2}DEM (Fig. 2). An example of C^{2}DEM conversion from a point cloud data is shown in Fig. 3.

Considering a path planning using the conventional DEM (with a square-shaped reference grid), a generated path on the conventional DEM always restricts the rover to change its heading of 45 degrees increments (Fig. 4-a). The path with such restriction may be suboptimal and requires the rover to make unnecessarily maneuvers. On the other hand, the C^{2}DEM has two remarkable improvements over the conventional DEM: the rover can head for any directions between -90 to 90 degrees with the step of angular resolution when starting from the initial position (at the origin of the map). Furthermore, as shown in Fig. 4-b, the heading angle of the rover from a current node to adjacent nodes varies with the reference grid shape, which enables the path planning to alleviate the above-mentioned restriction of the conventional DEM.

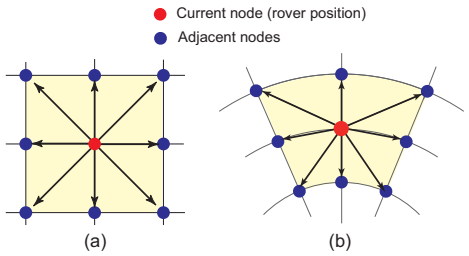

Figure 4. Possible headings (indicated by arrows) from the current node to adjacent nodes on the conventional DEM (a) and C^{2}DEM (b)

It should be noted that mapping approaches that are similar to the C^{2}DEM have been reported. For example, a log-polar grid map representation with an ultrasonic sensor has been proposed in [10]. A comparison between a local multi-resolution representation and a log-polar representation has been presented in [11]. Additionally, a hyperbolic polar coordinate map for infinitely long distance vision and path planning has been described in [12]. Compared to these previous studies, the C^{2}DEM is a fully three-dimensional map that can be applicable for path planning on rough terrain. Field experiments on the terrain mapping and path planning has validated the usefulness of the C^{2}DEM over the conventional DEM, as reported in [13].

3. PATH PLANNING AND NAVIGATION FOR ROUGH TERRAIN

Once the terrain feature map is provided, the rover performs a path planning to find a route for avoiding mobility hazards and to reach a designate location. There have been substantial studies dealing with path/motion planning algorithms for mobile robots, such as the A* and D* methods [14], the potential field approach [15], the probabilistic roadmap technique [16], and the rapidly-exploring random tree (RRT) algorithm [17]. The Mars Exploration Rovers have an autonomous navigation with hazard avoidance technology based on a local path planner called GESTALT [18]. The autonomous navigation system has been updated to achieve a simultaneous local and global path planning by the Field D* algorithm [19].

The path planning algorithm in this work uses a classical graph search algorithm (Dijkstra's algorithm) to generate a path from a start point to a goal point. A cost function used for the algorithm is composed of the three indices: terrain inclination, terrain roughness, and path length. Each index can be computed based on the C^{2}DEM representation. The least cost path obtained from the algorithm varies with the values of the weighting factors for the indices. In this paper, a multi-path planning method is also developed to address the arbitrariness of the values of the weighting factors and to find the most feasible path for travel.

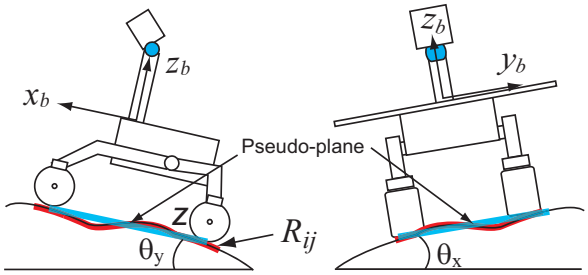

Figure 5. Terrain inclination angles. The red curvature depicts the projection region R_{ij} and the blue line depicts the pseudo-plane, which is composed of the wheel contact points.

3.1. Path Planning Algorithm

3.1.1. Terrain Inclination Index

A rover experiences relatively high wheel slippage when it climbs up or traverses on a sloped terrain. This slippage is due to the traction load from the gravity, which becomes significant on the sloped terrain. Additionally, rollover of a rover traversing on a steep slope is a mobility hazard. The terrain inclination index is employed for the cost function to represent such risks on a sloped terrain.

The terrain inclination index is divided into two axes, roll and pitch of the rover (Fig. 5). Each axis is geometrically calculated as an angle between the inertial coordinate and a pseudo-plane composed of the wheel contact points at a projection region of the rover R_{ij}: Multiple terrain inclinations can be calculated from each subset of three contact points between the multiple wheels. The terrain inclination index is the largest inclination between these values:

$$\begin{aligned} \text{Roll} &: \Theta_{xij} = \max(\theta_x(R_{ij})) \\ \text{Pitch} &: \Theta_{y_{ij}} = \max(\theta_y(R_{ij})) \end{aligned} \tag{1}$$

The projection region R_{ij} is determined with the dimension of the rover. The heading direction is aligned along with the vector $\overrightarrow{n}_{ij}$, which is composed of the current node n_i and adjacent node n_j (Fig. 6).

3.1.2. Terrain Roughness Index

The terrain roughness is related to the traversability of a rover. To avoid uneven bumpy areas for travel path, the terrain roughness index B_{ij} is employed. First, the nodes inside the projection region R_{ij} are rotated around the x and the y with Θ_{xij} and $\Theta_{y_{ij}}$, such that the nodes are represented in the terrain coordinate system. The terrain roughness is then calculated as the standard deviation of the local elevations z' at the terrain coordinate [20]:

$$B_{ij} = \sqrt{\frac{1}{N} \sum_{n_k \in R_{ij}} \left(z'_k - \bar{z'}(R_{ij})\right)^2} \tag{2}$$

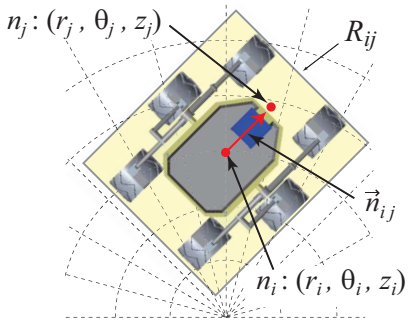

Figure 6. Projection region (yellow-colored area) of the rover on a terrain map.

where N represents the number of nodes inside the region and $\bar{z'}$ denotes the average elevation in R_{ij}. Rougher terrains around a node increase the index at the node.

3.1.3. Path Length Index

The path length index is used to find the shortest path from a start point to a goal point. The path length index L_{ij} is the distance from the current node n_i to adjacent nodes n_j:

$$L_{ij} = \sqrt{r_i^2 + r_j^2 - 2r_i r_j(\cos(\theta_i - \theta_j)) + (z_i - z_j)^2} \tag{3}$$

3.1.4. Cost Function for Path Planning

A cost function for path planning is defined by the following equation that is comprised of the above-mentioned indices:

$$C(\boldsymbol{p}) = \sum_{n_i \in \boldsymbol{p}} \left(W_{\theta_x} \frac{\Theta_{xij}}{N_{\theta_x}} + W_{\theta_y} \frac{\Theta_{yij}}{N_{\theta_y}} + W_B \frac{B_{ij}}{N_B} + W_L \frac{L_{ij}}{N_L} \right) \tag{4}$$

where W_{θ_x}, W_{θ_y}, W_B, and W_L are the weighting factors, which assign specific priorities to the corresponding indices. The weighting factors for the terrain inclination indices have a value of infinity if the indices exceed predetermined threshold angles. The threshold angles are determined based on the slope traversability of the rover (i.e., maximum slope climbing angle). N_{θ_x}, N_{θ_y}, N_B, and N_L are the normalization factors. Each factor is the maximum value of the corresponding index calculated from the terrain map. The path $\boldsymbol{p}$ consists of a series of neighboring/chained nodes:

$$\boldsymbol{p} = \{\underbrace{n_{start},\ \cdots,\ n_i,\ n_j,\ \cdots,\ n_{goal}}_{N_p}\} \tag{5}$$

The cost function in Eq. (4) indicates the difficulty of the terrain traversability. Smaller index values result in lower mobility hazard levels on a path. Therefore, the path planning problem is a least-cost search problem. The conventional Dijkstra's algorithm is used in this work to find the least-cost path, providing a minimum value for the cost function.

3.2. Multi-Path Planning and Evaluation Method

The least-cost path provided by Eq. (4) varies in accordance with the values of the weighting factors for the individual indices. For example, larger weighting for the path length generates shorter path, but possibly induces more chances for mobility hazard. On the other hand, larger weightings for the terrain inclination reduce the mobility hazard levels on the path, but increase the length of the path, requiring larger energy consumption in total. Thus, the problem is how to determine the values of the weighting factors with respect to the rover mobility. Additionally, generated paths with different values of the weighting factors should be evaluated based on a metric that includes the path cost and the possibility of mobility hazard.

The current work in this paper considers the following approach to find the values of the weighting factors that provide the most feasible path: first, a number of different sets of the weighting factors are given to Eq. (4), providing multiple number of "candidate" paths on a terrain map. Subsequently, the candidate paths are quantitatively examined based on an evaluation metric. The following equation is defined for the evaluation metric of the path $\boldsymbol{p}_k$ with the set of weighing factors $\boldsymbol{W}_k$:

$$\begin{aligned} E(\boldsymbol{p}_k) &= \frac{C(\boldsymbol{p}_k)}{N_p(\boldsymbol{p}_k)} + \frac{D(\boldsymbol{p}_k)}{\bar{D}} \\ &+ \frac{\max(\theta_x(\boldsymbol{p}_k))}{\hat{\theta}_x} + \frac{\max(\theta_y(\boldsymbol{p}_k))}{\hat{\theta}_y} \end{aligned} \tag{6}$$

where D is the length of the path, $\bar{D}$ is the average path length between the candidate paths, and N_p is the number of the nodes on the path. $\max(\theta_x)$ and $\max(\theta_y)$ are the maximum terrain inclination at the path. $\hat{\theta}_x$ and $\hat{\theta}_y$ are the threshold angles for the terrain inclination. The first term in Eq. (6) is the average cost required for the rover to move through consecutive nodes. The second term indicates the ratio for the path length. The third term implies a rollover possibility w.r.t. the threshold angle for the roll axis. The fourth term is a stall possibility w.r.t. the threshold angle for the pitch axis while the rover climbing a sloped terrain. Calculating the evaluation metrics for all candidate paths, the most feasible path between them is determined such that the path has the minimum value of the evaluation metric.

Compared to the heuristic approach such as RRT, the proposed method uses a deterministic path selection: first, multi-path planning is performed with varied weighting factors and provides candidate paths; and then, the most feasible paths with appropriate values of the weighing factors, that can minimize the evaluation metric, can be found.

3.3. Navigation Command

The most feasible path is discretized into several way points. A navigation command, consisting of the relative distance and heading from one way point to the next, can

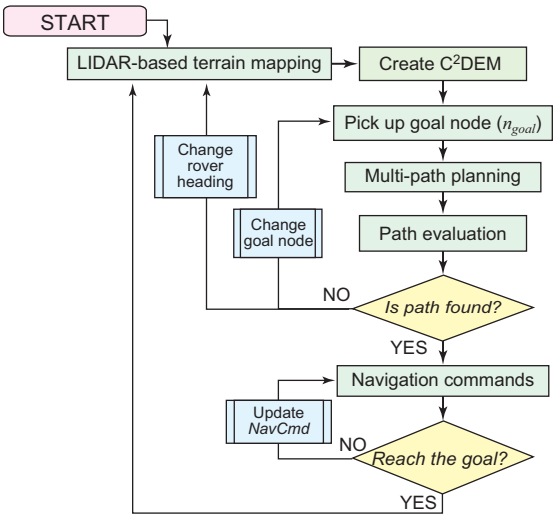

Figure 7. Flowchart of the autonomous mobility with LIDAR-based terrain mapping and path planning

be geometrically calculated based on the terrain map data. Then, the rover mobility executes the sequential navigation commands from a start point to a goal point so that it travels through each way point.

In the experiments described in Section 4, a baseline technique for the positioning is done by a wheel odometry while a visual odometry is partially used to compensate an errors due to wheel slippages. An inertial reference unit with gyroscopes is also used for the measurement of the heading and orientation of the rover.

3.4. Procedures for Autonomous Mobility

The autonomous mobility with the LIDAR-based terrain mapping, the multi-path planning, and the navigation are summarized as follows (Fig. 7):

1. The rover executes the LIDAR-based terrain mapping and obtains the point cloud data of the terrain.
2. The point cloud data are converted to the C^2DEM.
3. A rover operator selects a desired goal node located inside of the C^2DEM.
4. The multi-path planning with different sets of weighting factors are performed to provide candidate paths from a rover position (origin of the map) to the goal node.
5. The candidate paths are examined based on the evaluation metric and the most feasible path between them is selected. If the metric of the path exceeds a predefined threshold, the goal node is changed to re-plan a path, or the rover changes its heading and scans a new terrain for an alternative path planning.
6. Once the feasible path is found, the rover starts navigating itself through the consecutive way points until the rover reaches the goal.
7. The rover repeats the above-mentioned tasks to extend its exploration area.

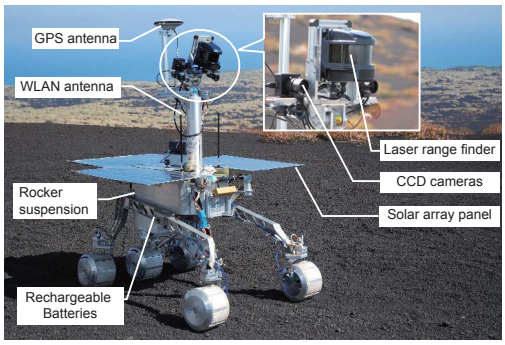

Figure 8. Rover test bed:Micro-6

4. FIELD EXPERIMENTS

Field experiments with a rover test bed were performed at a Lunar/Martian analog field (Izu-Oshima Island, Japan) to evaluate the usefulness of the proposed techniques. The terrain in the field is mostly covered with scoria, scattered rocks and stones. The test field also consists of sloped terrain, ditches, and vegetations.

In the experiment, the multi-path planning and evaluation method is tested in specific scenarios. The autonomous mobility with the proposed techniques is then demonstrated in a long-range navigation scenario.

4.1. Rover Test Bed Overview

Micro-6 (Fig. 8) is the rover prototype developed by the authors to demonstrate the mobility and navigation on rough terrain and power management control. The rover has a 4-wheeled drivable/steerable unit that DC brushed motors actuate. The left and right wheel pairs are connected via a non-spring passive rocker-link suspension, which shows a good traversability in rough terrain. The rover has two stereo camera pairs and the LIDAR for obstacle recognition and terrain mapping. These are mounted on the gimbals that can rotate ± 120 degrees in the tilt (around the pitch axis) and ± 180 degrees in the pan (around the yaw axis). The power management subsystem provides electrical power for the rover via the solar array panels with rechargeable batteries. The communication between the rover and its operators is handled via a wireless LAN in 2.4 GHz band. Detail descriptions of the rover subsystems were presented in [21].

During the tests, a wheel odometry was used to determine the rover position (relative displacement) while a visual odometry with the onboard camera was also partially exploited to compensate the wheel odometry errors due to the wheel slippages. The rover orientation was measured by an attitude and heading reference system. The GPS antenna mounted on the rover also measured the rover position as a ground truth to evaluate the rover trajectory afterwards the experimental tests. The GPS measurement achieves an accuracy of a few centimeters with post-processed kinematic computation.

Table 2. Weighting factors for the multi-path planning

Path	W_B	W_{θ_x}	W_{θ_y}	W_L
Path A	0.10	0.00	0.00	0.90
Path B	0.10	0.05	0.05	0.80
Path C	0.10	0.10	0.10	0.70
Path D	0.10	0.15	0.15	0.60
Path E	0.10	0.20	0.20	0.50
Path F	0.10	0.25	0.25	0.40
Path G	0.10	0.30	0.30	0.30
Path H	0.10	0.35	0.35	0.20
Path I	0.10	0.40	0.40	0.10
Path J	0.10	0.45	0.45	0.00

4.1.1. Multi-Path Planning and Evaluation Tests

Based on the scheme for the multi-path planning and evaluation method, 10 sets of the weighting factors are given in the experiment, which can generate 10 different types of candidate paths. The constraints given to these sets are as follows: $W_B + W_{\theta_x} + W_{\theta_y} + W_L = 1.0$, $W_{\theta_x} = W_{\theta_y}$, and $W_B = 0.1$. Tab. 2 summarizes the weighting factors used in the experiments. The weighting factor for the path length was varied from 0.0 to 0.9 with the step of 0.1, while the weighting factors for the terrain inclination were varied such that W_{θ_x} (or W_{θ_y}) $= (1.0 - W_B - W_L)/2.0$. It is expected that Path A will be the shortest but may remarkably include mobility hazard, whereas Path J will have less mobility hazard and provide the longest path length between the candidate paths. The threshold angle for the terrain inclinations is set as 10 degrees.

The scenarios considered in the tests are 1) obstacle avoidance and 2) ditch crossing maneuvers. Each maneuver has been tested on different types of terrain conditions (i.e. different obstacle sizes and locations, or different width/depth of ditch), and typical results among them are presented in this paper.

Fig. 9 illustrates the result of the multi-path planning in an obstacle avoidance scenario. It can be clearly seen from the figure that different types of candidate paths were generated for the obstacle avoidance maneuver because of the variety of the weighting factors: Path A $\sim$ Path G traversed on the left side (upslope) of the obstacles while Path H was on the right side (downslope); Path I and Path J drew an S-shaped curve to avoid the obstacles.

Fig. 10 summarizes the quantitative characteristics of each path: the distance ratio (blue bars in the figure) increases as W_L decreases; the rollover possibility (green bars) and the stall possibility (red bars) decreases with increasing W_{θ_x} and W_{θ_y}. From the figure, the most feasible path, which has the minimum value of the evaluation metric, was determined as Path H because the distance ratio was relatively short and the rollover/stall possibilities are not remarkable.

Fig. 11 shows the result of the multi-path planning in a ditch crossing scenario. From the figure, Path A traveled relatively steep area of the ditch, and therefore, the terrain inclinations of the path were very close to their threshold values (10 degrees), providing the largest value for the evaluation metric. Path J largely bypassed the ditch, resulting in the longest path length. The evaluation metrics of the candidate paths are illustrated in Fig. 12. In this scenario, the most feasible path was determined as Path B with the minimum value of the evaluation metric.

From the experimental tests, it can be seen that an appropriate set of the weighting factors, which provide the most feasible path, varies along with the terrain characteristics (obstacles, roughness, ditches, and others); the most feasible path is not always a shorter path, nor a path with less terrain inclination. Therefore, the weighting factors should be dynamically tuned with respect to these terrain characteristics. The results here indicate that the proposed method for the multi-path planning and evaluation can adaptively produce a feasible path on any different types of terrain characteristics.

4.1.2. Long-range Navigation Tests

The long-range navigation test was performed three times with different types of terrain. A typical result among these tests is shown in Fig. 13. The rover executed terrain mapping, path planning and navigation at multiple intermediate goals (20 in total), and successfully traveled 0.31 km in approximately three hours. The top section of Fig. 13 illustrates that the rover evaded several obstacles (bushes) throughout the terrain, and selected feasible paths toward each intermediate goal. It should be noted that the rover had to backtrack along the path at the 5th intermediate goal due to the following reasons: the rover could not find a feasible path because the terrain was so rocky that the evaluation metric of the path exceeded the predefined threshold. Additionally, the rover needed to head north to obtain enough sunlight for the solar array panels to recharge the batteries.

5. CONCLUSIONS AND FUTURE WORK

This paper has described the LIDAR-based terrain mapping and multi-path planning method that is used for an autonomous mobility of a planetary exploration rover. The main contribution of this works is the development and practical implementation of the following two key features: the terrain mapping with the C^2DEM which achieves detailed representation of the terrain near the rover. The other is the multi-path planning and evaluation method that performs extensive exploration of the weighting factors to obtain the most feasible path. The field experiment with the rover test bed at the Lunar/Martian analog site validated the usefulness of the proposed techniques.

The future work of this study includes an online augmentation of consecutive terrain maps that will enable the rover to execute a global path planning. The LIDAR sen-

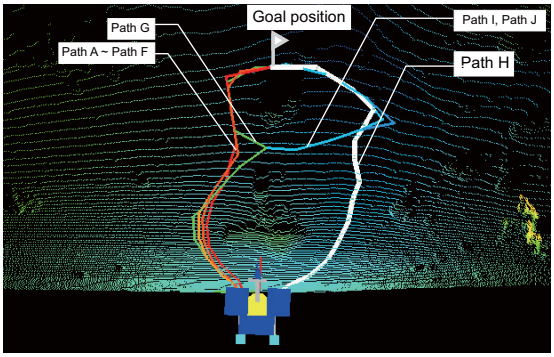

Figure 9. Experimental results for the multi-path planning: Obstacle avoidance maneuver (the path with a white bold line depicts the most feasible path between the candidates)

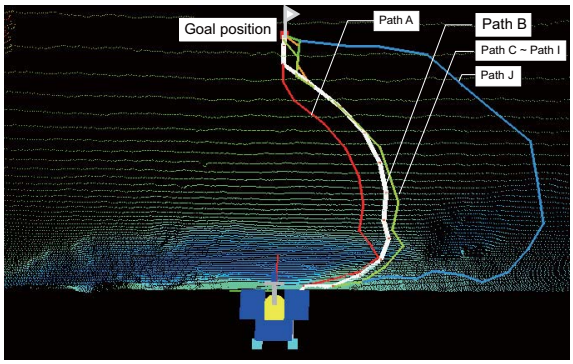

Figure 11. Experimental results for the multi-path planning: Ditch crossing maneuver (the path with a white bold line depicts the most feasible path between the candidates)

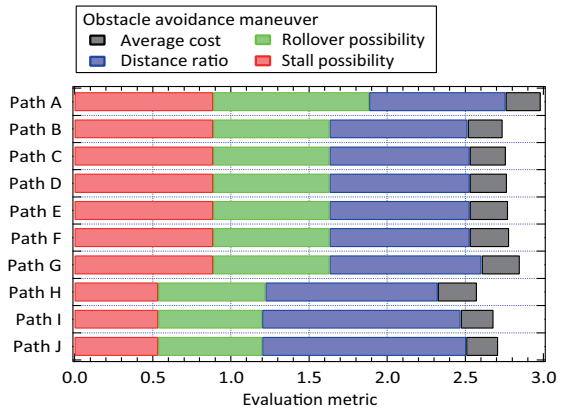

Figure 10. Calculation result of the evaluation metrics for candidate paths: Obstacle avoidance maneuver

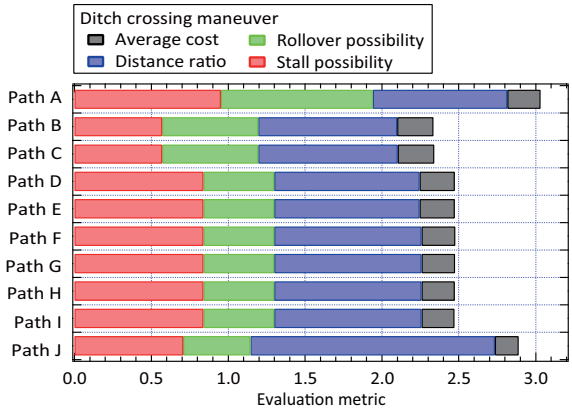

Figure 12. Calculation result of the evaluation metrics for candidate paths: Ditch crossing maneuver

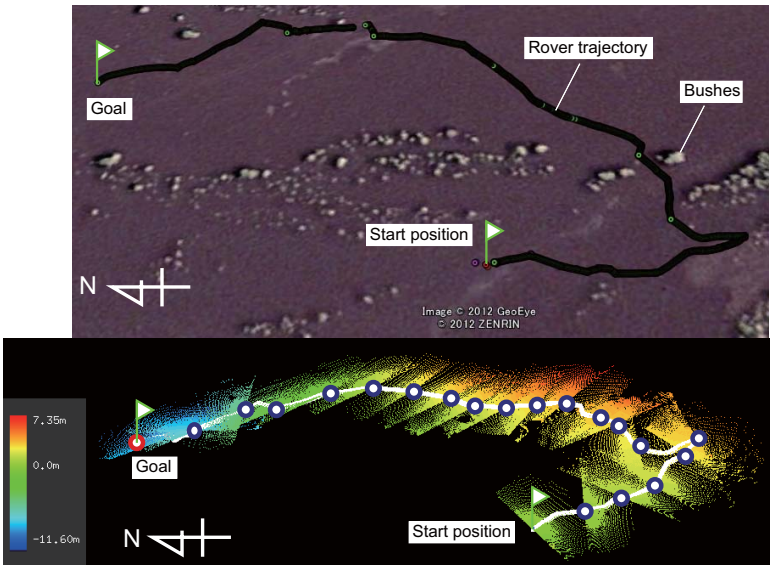

Figure 13. Long-range navigation: The upper figure shows an overview of the rover trajectory, plotted on Google Earth. The red circle in the lower figure depicts the final goal and the blue circles depict the intermediate goals.

sor used in this work involves a scanning mechanism with an actuator and movable parts, that may be less durable for launch vibrations and landing shocks. Alternatively, a 3D flash LIDAR imaging system is being developed that achieves relatively fast capturing of 3D terrain mapping without any actuators and movable parts.

A drawback of the LIDAR-based mapping is that the LIDAR cannot obtain pure color data of the terrain (in grayscale or RGB) even though it can measure the distance as well as intensity of the light reflected from objects. Therefore, a possible future direction of this research may be to incorporate the LIDAR data with a single camera that enables three-dimensional mapping with texture information of terrain.

REFERENCES

[1] Matthies, L. (1992). Stereo Vision for Planetary Rovers: Stochastic Modeling to Near Real-Time Implementation. *Int. Journal of Computer Vision*, 8(1):71–91.

[2] Goldberg, S., Maimone, M., & Matthies, L. (2002). Stereo Vision and Rover Navigation Software for Planetary Exploration. In *Proc. of the IEEE Aerospace Conf.*, Big Sky, MT, pp. 5-2025–5-2036.

[3] Maimone, M., Johnson, A., & Cheng, Y. (2004). Autonomous Navigation Results from the Mars Exploration Rover (MER) Mission. In *Proc. of the 9th Int. Symp. on Experimental Robotics*, Singapore, pp. 3–13.

[4] Matthies, L., Maimone, M., Johnson, A., Cheng, Y., Willson, R., Villalpando, C., Goldberg, S., & Huertas, A. (2007). Computer Vision on Mars. *Int. Journal of Computer Vision*, 75(1):67–92.

[5] Wulf, O. and Wagner, B. (2003). Fast 3D Scanning Methods for Laser Measurement Systems. In *Proc. of the Int. Conf. on Control Systems and Computer Science*, Bucharest, Romania, pp. 312–317

[6] Thrun, S., Thayer, S., Whittaker, W., Baker, C., Burgard, W., Ferguson, D., Hahnel, D., Montemerlo, M., Morris, A., Omohundro, Z., Reverte, C., & Whittaker, W. (2004). Autonomous Exploration and Mapping of Abandoned Mines. *IEEE Robotics & Automation Magazine*, 11(4):79–91.

[7] Buehler, M., Iagnemma, K., & Singh, S., editors (2005). *The 2005 DARPA Grand Challenge: The Great Robot Race, Springer Tracts in Advanced Robotics (STAR) Series, Vol. 36*. Springer-Verlag Berlin Heidelberg.

[8] Buehler, M., Iagnemma, K., & Singh, S., editors (2009). *The DARPA Urban Challenge: Autonomous Vehicles in City Traffic, Springer Tracts in Advanced Robotics (STAR) Series, Vol. 56*. Springer-Verlag Berlin Heidelberg.

[9] UTM-30LX, Hokuyo Automatic CO. LTD (2012). Online at *http://www.hokuyo-aut.jp/* (as of 30 June 2012).

[10] Longega, L., Panzieri, S., Pascucci, F., & Ulivi, G. (2003). Indoor Robot Navigation using Log-polar Local Maps. In *Preprint of the 7th Int. IFAC Symp. on Robot Control*, Wroclaw, Poland.

[11] Nieuwenhuisen, M., Steffens, R., & Behnke, S. (2011). Local Multiresolution Path Planning in Soccer Games Based on Projected Intentions. In *Proc. of Robocup Int. Symp.*, Istanbul, Turkey.

[12] Sermanet, P., Hadsell, R., Scoffier, M., Muller, U., & LeCun, Y. (2008). Mapping and Planning under Uncertainty in Mobile Robots with Long-Range Perception. In *Proc. of the 2008 IEEE/RSJ Int. Conf. on Intelligent Robots and Systems*, Nice, France, pp. 2525–2530.

[13] Ishigami, G., Otsuki, M., & Kubota, T. (2012). Path Planning and Navigation Framework for a Planetary Exploration Rover using a Laser Range Finder. In *Proc. of the 8th Int. Conf. on Field and Service Robots*, Matsushima, Japan.

[14] Stentz, A. (1994). Optimal and Efficient Path Planning for Partially-known Environments. In *Proc. of the 1994 IEEE Int. Conf. on Robotics and Automation*, San Diego, CA, pp. 3310–3317.

[15] Barraquand, J., Langlois, B., & Latombe, J. (1992). Numerical Potential Field Techniques for Robot Path Planning. *IEEE Transaction on Systems, Man and Cybernetics*, 22(2):224–241.

[16] Kavraki, L. E., Svestka, P., Latombe, J.-C., & Overmars, M. H. (1996). Probabilistic Roadmaps for Path Planning in High-dimensional Configuration Spaces. *IEEE Transaction on Robotics and Automation*, 12(4):566–580.

[17] Cheng, P., Shen, Z., & Lavalle, S. M. (2001). RRT-Based Trajectory Design for Autonomous Automobiles and Spacecraft. . *Archives of Control Sciences*, 11(3-4):167–194.

[18] Biesiadecki, J. and Maimone, M. (2006). The Mars Exploration Rover Surface Mobility Flight Software: Driving Ambition. In *Proc. of the 2006 IEEE Aerospace Conf.*, Big Sky, MT.

[19] Carsten, J., Rankin, A., Ferguson, D., & Stentz, A. (2008). Global Planning on the Mars Exploration Rovers: Software Integration and Surface Testing. *Journal of Field Robotics*, 26(3):337–357.

[20] Iagnemma, K. and Dubowsky, S. (2004). *Mobile Robots in Rough Terrain: Estimation, Motion Planning, & Control with Application to Planetary Rovers*. Springer-Verlag Berlin Heidelberg.

[21] Otsuki, M., Ishigami, G., Shimada, T., Takanashi, S., Ann, O., & Kubota, T. (2011). Experimental Study on Mobility and Navigation for Exploration Rover in Natural Rough Terrain. In *Proc. of the 28th Int. Symp. on Space Technology and Science*, Okinawa, Japan, d-87p.